A&A manuscript no.
(will be inserted by hand later)

Your thesaurus codes are:
13.25.5 08.03.5 08.12.1

ASTRONOMY
AND
ASTROPHYSICS
9.9.1996

Coronal Properties of Nearby Old Disk and Halo dM Stars

G. Micela[1], J. Pye[2], and S. Sciortino[1]

[1] Istituto e Osservatorio Astronomico di Palermo, Palazzo dei Normanni, 90134 Palermo, Italy
[2] Department of Physics and Astronomy, University of Leicester, Leicester, LE1 7RH, UK

Received date 1996, accepted date

Abstract. ROSAT X-ray (PSPC) and EUV (WFC) observations of a sample of 12 nearby Halo and Old-Disk low mass stars have been analyzed to determine their emission levels, properties of their coronal spectra and to characterize their temporal variations on time scales from hours to ten years. The light curves of the old-disk stars of our sample with the highest count statistics, show that variability of a factor two on a time scale of a few thousands of seconds is a common property of old-disk stars. The coronal emission of GJ 191, the only halo star with enough counts to make the time analysis feasible, shows significant variations on a time scale of six months.

The time resolved spectral analysis of the most intense stars shows that their coronal emission is consistent with a two temperature model with (approximately) constant values of the temperatures along the entire observation, while the observed variability can be explained by changes in their emission measure distributions. We find that the emission measures of the two components change coherently during the observations.

For all ten detected stars we have computed hardness ratio and X-ray luminosity. While our old-disk stars fit well in the body of the distribution outlined by a complete volume limited sample of dM and dK stars within 7 pc (Schmitt et al. 1995), the halo stars tend to occupy the softest and weakest envelope defined by population I low-mass stars.

Key words: Stars: activity – Stars: coronae – Stars: late-type – X-rays: stars

1. Introduction

X-ray data obtained with the *Einstein Observatory* have brought a major change in our perception of stellar coronae as a result of the observation of X-ray emission from normal stars throughout the H-R diagram. The presence of coronae, and the operation of associated non-radiative heating mechanisms, have been shown to be the rule rather than the exception (see Vaiana et al., 1981; Rosner et al., 1985; Linsky 1985; Pallavicini 1989; Sciortino 1993). Past detailed studies of the physical properties characterizing the plasma responsible for stellar X-rays based on a few selected samples of a small number of stars (Mewe et al., 1982; Vaiana 1983; Majer et al., 1986; Stern et al., 1986; Schmitt et al., 1987) have led to the recognition that such plasma may have several temperature components – consistent with a continuous distribution of emission measure from plasma over an ample range of temperatures, that the photon spectrum depends on the activity of the stars, and that there is indication of a correlation between X-ray luminosity and coronal temperature.

A complete survey of the coronal X-ray temperature of late-type stars as observed with the *Einstein* Imaging Proportional Counter (Schmitt et al., 1990) has allowed investigation of the physical parameters of stellar coronae across the H-R diagram. The sample of 130 stars extracted from the Woolley and the BSC catalogues constitutes the largest data base available to date analyzed in an uniform way. This detailed spectral analysis has shown that the frequently found one (1-T) and two temperature (2-T) descriptions are heavily influenced by the signal-to-noise ratio of the data and by the spectral resolution of the instrument. The comparison of Einstein and EXOSAT measurements indicates the existence of multi-temperature components in coronal plasmas (Pallavicini et al., 1988). The emission measure distribution, as result from the analysis of IPC spectra, shows intrinsic differences between four groups of stars, namely: dwarf F and G stars, dwarf M stars, yellow giants, and RS CVn systems. In general, dwarf M-star spectra, when gathered with sufficient signal-to-noise ratio, show evidence for both high-temperature gas ($T > 10^7$ K) and lower temperature ($T \sim 3 \cdot 10^6$ K) gas, while dwarf F and G stars have weak (or absent) high-temperature component with the notable exception of young stars (Stern et al. 1986, Güdel et al. 1995, 1996). As a group, RS CVn systems show evidence for extremely hot coronae ($T > 10^{7.5}$ K), sometimes

Send offprint requests to: G. Micela

with no accompanying lower temperature plasma. Indeed the analysis of the spectra of a sample of active binaries observed with the ROSAT PSPC shows that a cool component ($T \sim 2 \cdot 10^6$ K) is always present but with a low emission measure (Dempsey et al. 1993). The majority of the surveyed giant stars shows a very hot corona ($T > 10^7$ K), but without the lower temperature component characterizing the dwarf stars, although this last result has been refuted by ROSAT observations of other giants (Maggio et al., 1994). This IPC based spectral survey – while the source of a remarkable wealth of information – had several limitations. To begin with, due to the approximately flux limited nature of the Einstein observations, essentially all the stars with available spectra have X-ray luminosities above the median for their class. Likely, this introduces a bias preventing the ready extension of the spectral survey results to fainter X-ray coronal sources.

The direct comparison of the X-ray luminosity functions (as deduced by the *Einstein* Observatory) of several coeval stellar samples, such as the Pleiades, the Hyades, and the disk population dwarfs has shown the decay of X-ray luminosity level with increasing stellar age (Vaiana, 1983; Micela et al. 1985; 1988; 1990; Feigelson and Kriss 1989). This result has recently been confirmed by available ROSAT data of various coeval stellar samples (see for example, Patten & Simon 1993; Pye et al. 1994; Stauffer et al. 1994; Randich & Schmitt 1995; Randich et al. 1995a, 1995b; Stern et al. 1995; Micela et al. 1996)

The analysis of *unbiased* samples of nearby dwarf K and M field stars (Barbera et al. 1993) observed with *Einstein*, has shown that young disk dwarf K and M stars have mean X-ray luminosity greater than old disk ones. Barbera et al. have also found hints that halo K and M stars have X-ray luminosity still fainter than old disk stars. Recently a complete survey of X-ray emission of dK and dM stars inside 7 pc has been performed by Schmitt et al. (1995) with ROSAT observations. Fleming et al. (1995), using those data, fail to find differences between the X-ray luminosity distribution of kinematically young and old dM stars, while finding a different behavior between metal poor and metal rich stars concluding that abundance is a better indicator of age than kinematical velocity.

Moreover, by comparing the hardness ratios of Pleiades, Hyades, and nearby disk population dG stars, Micela(1991) has suggested the softening of the coronal X-ray spectrum with increasing stellar age. The detailed fits of ROSAT and ASCA spectra of a sample of 12 G0-G5V stars covering the range log(age)=7.8-10 have shown the decrease both of the fitted high temperature and of its emission measure with respect to the low temperature one with increasing stellar age (Güdel et al., 1996) reinforcing the early Einstein IPC findings based on the analysis of hardness ratios. A search for similar behaviour in a sample of nearby K and M stars is the main aim of the present paper. Fleming et al. (1995) found that metal rich stars have a harder spectrum than metal poor stars. However they do not discuss in detail the few halo stars present in their sample, with respect to the disk population stars.

In order to characterize the change of coronal spectra with stellar age, in particular for the low X-ray luminosity old disk and halo low-mass stars, long exposure times (much longer than those allowed for the exploratory nature of *Einstein* observations) with the ROSAT PSPC detector, are required. A proper exploration of the age and L_x parameter space requires an accurate selection of the target stars and prevents this scientific objective being pursued using only all-sky survey data (RASS).

Using available *Einstein* IPC data it has been possible (Schmitt et al., 1990) to perform meaningful spectral fits only for the old disk dK5 star Gliese 845. The derived coronal temperature and X-ray luminosity of this star are the lowest among the stars of similar spectral type.

The investigation of X-ray luminosity level and spectra of halo and old stars, has important consequences not only on our present understanding of coronal physics, addressing problems such as the aging of the coronal heating mechanism, and/or the relation of coronal emission with atmosphere chemical composition, but is also relevant to the determination of the spectral shape of the stellar contribution to the soft X-ray background (Micela 1991; Micela et al., 1991; Kashyap et al., 1992). The lack of detailed X-ray spectral information of old disk and halo population stars, makes these predictions still uncertain. The spectral information on the halo and old disk stars will permit a more accurate modeling particularly valuable for future missions such as AXAF and XMM.

Finally, we note that combining Einstein IPC and ROSAT PSPC data allows us to address questions related to long term variability of X-ray intensity and perhaps of the coronal spectrum. In addition, long ROSAT exposures should furnish valuable data to study the occurrence of variability on time scales of a few days.

Our paper is organized as follows: in §2 we describe the sample selection and the X-ray observations, in §3 we present timing properties of X-ray emission of stars in our sample, in §4 their spectra, in §5 we discuss our results and their implications, and finally in §6 we summarize our main conclusions.

2. The observations

2.1. The selected sample

The nucleus of our sample derives from five halo (H) and old disk (OD) stars observed by ROSAT in a dedicated observing program we proposed to pursue the scientific objectives outlined above. We have added to this original sample all stars observed with the ROSAT PSPC available in the public archive at February 1995 classified as H or O/H from Leggett (1992) in her study of low-mass stars. This classification is based both on kinematical and photometric criteria making us confident about its reliability.

After having excluded the stars GJ 513 and GJ 1062 since they were completely obscured by the circular rib of the PSPC, we were left with 7 O/H or H and 4 OD dM stars. All stars have been observed once in the center of field of view, except the stars GJ 191 and GJ 406 observed twice from different observers.

Table 1 summarizes the optical and kinematical characteristics of selected stars as listed in the CNS3 catalog and indicates if the star has been observed with the *Einstein* IPC.

Table 1. Optical Properties of Selected Sample

Name GJ	Dist [pc]	m_V	Sp. Type	POP.	IPC Obs	Other name
1	4.51	8.54	M4	H	No	HD225213
191	3.87	8.85	M0	H	Yes	Kapteyn Star
213	6.01	11.53	M4	O/H	Yes	Ross 47
299	6.76	12.83	M5	H	No	Ross 619
398	13.7	12.60	M4	OD	Yes	RY Sex
406	2.39	13.45	M6	OD	Yes	CN Leo
595	9.01	11.87	M3.5	H	No	
699	1.83	9.55	M5	O/H	Yes	Barnard Star
821	10.8	10.87	M3	H	No	Wolf 918
845	3.44	4.69	K4e	OD	Yes	ϵ Ind
866	3.40	12.66	M5e	OD	Yes	EZ Aqr
887	3.52	7.34	M2e	OD	Yes	HD217987

2.2. X-Ray and EUV data

Table 2 summarizes the main characteristics of the ROSAT X-ray observations. For each star we have evaluated the number of counts in a circular region of 2' of radius, while the background is measured in an annulus centered on the source position with internal and external radii of 2.5' and 3.0', respectively. For the star GJ 595 we have used a circular region masked with two pie cuts to exclude the contribution of two nearby intense sources. For the stars detected at above the 3σ level we have adopted the position of the centroid of the photons in the energy range (0.2-2.4) keV, while for undetected stars we have used the optical positions from the CNS3 catalog precessed to J2000 and corrected for proper motion at 1990 epoch. Net counts and rates in the table refer to the (0.14-2.4) keV bandpass; we have not used the softer energy channels since at lower energies the instrument suffers from an electronic 'ghost image' problem affecting the spatial distribution of the softest photons (Nousek & Lesser 1993).

We have searched for EUV detections of all our sample stars in the WFC all-sky survey data, using the PSS (Point Source Search) program within the UK Starlink ASTERIX data analysis package. We have also used PSS on the pointed-phase WFC data (obtained simultaneously with the PSPC data) for the five stars with the highest PSPC count rates (GJ 398, 406, 845, 866, 887; see Table 2). All the pointed observations were obtained in the S2-band, while the survey provided data in both the S1-band (60–140 Å) and S2-band (112–200 Å) (see eg. Pye et al. 1995). Since we were only interested in detections within ~ 2 arcmin of the known, optical positions of the stars, the source search was conducted down to a relatively low significance threshold of 3σ.

The EUV results are summarized in Table 3. All the count rates have been corrected to on-axis, 'at-launch' values (cf. Pye et al. 1995, section 4.3). Four of our stars were detected, in a total of six observations. Only one of the stars, GJ 406 (= CN Leo) was reported in the WFC 2RE Catalogue (Pye et al. 1995). GJ 398 and GJ 866 were not detected in the pointed data, but examination of the upper limits to their count rates shows that this is not surprising. The all-sky survey observations were made during the period 1990 July to 1991 January; the dates of the pointed observations are given in Table 2. The survey and pointed S2-band count rates of GJ 406 are consistent. The survey S1-band count rate and pointed S2-band count rate of GJ 845 are also consistent, given the proximity (and hence low absorption column) of the star.

It is useful to compare the observed count-rate ratios (WFC-S1 / WFC-S2, PSPC / WFC-S1, PSPC / WFC-S2) with ranges predicted on the basis of simple assumptions, as extreme values might indicate time variability (between the two measurements) or an anomalous spectrum. We assume an isothermal, optically-thin (Raymond–Smith) spectrum with photoelectric absorption. For $0.1 \lesssim T \lesssim 1.0$ keV and $n_H \lesssim 10^{18}$ cm^{-2}, the predicted ratios PSPC : WFC-S1 and PSPC : WFC-S2 are in the range $\sim$ 10–50; these ratios increase with n_H. For $0.1 \lesssim T \lesssim 1.0$ keV and $10^{18} \lesssim n_H \lesssim 10^{19.5}$ cm^{-2}, the predicted ratio WFC-S1 : WFC-S2 is in the range $\sim$ 0.3–4; this ratio also increases with n_H. For example, GJ 406 has a PSPC : WFC-S2 ratio of $\approx$ 10 or 30 depending on whether we take the PSPC count rate from sequence 201722 or 201577 respectively (cf. Sect. 3.2). Indeed, Wood et al. (1994) and McGale et al. (1995) note the presence of a flare (duration $\lesssim 1.5$ hours) in the WFC S2-band survey data, with a count rate of ~ 0.35 count/s averaged over 1.5 hours (see McGale et al. 1995, figure A1); removing this enhancement would roughly halve the estimate of the time-averaged count rate.

3. Time Variability in X-ray ROSAT observations

For each of the detected stars, except GJ 398 (observed with a very short exposure time), we have obtained light curves in the (0.11-2.4) keV passband. All stars observed with enough statistics show variations with amplitude up to a factor 2-3 on a time scale larger than a few thousand seconds. In general we are unable to constrain the characteristics of the variability because of the temporal gaps inside each observation. In the following we discuss in de-

Table 2. Characteristics of X-ray Observations

GJ	Obs.seq.	PI[1]	Exp.Time (s)	Obs. Start MJD	Net Counts	Count rate (ct/ks)	Percentage Error
1	201008	Hawley	4808	48956.35	100.3	20.86	17.5
191[2]	200523	Hawley	14994	48712.44	438.8	29.27	7.5
191[2]	201105	Schmitt	3056	48894.71	184.9	60.50	9.5
213	201338	Micela	14026	48886.92	101.4	7.23	17.5
299	200129	Giampapa	7359	48356.79	<41.8	< 5.68	...
398	201724	Micela	204	49325.72	47.6	233.33	16.3
406[2]	201577	Schmitt	1493	49325.91	1495.5	1001.67	4.0
406[2]	201722	Micela	2684	49325.98	718.2	267.59	2.7
595	201006	Hawley	9282	48854.39	<48.6[3]	< 5.24	...
699	200128	Giampapa	4515	48318.20	105.4	23.34	17.0
821	201007	Hawley	18215	49102.82	120.7	6.63	23.5
845	200559	Bookbinder	14798	48750.80	8560.6	578.50	1.1
866	201723	Micela	13203	49328.07	4324.2	327.52	1.6
887	201339	Micela	13588	49142.05	3134.1	230.65	2.0

[1] Principal Investigator of original proposal
[2] This star has been observed twice from different observers.
[3] The counts of this source have been evaluated in a circular region masked for eliminating the contribution of two nearby sources. The quoted upper limit is corrected for the masked area.

Table 3. ROSAT EUV results for the sample stars. The detection threshold is 3.0σ. The counts and count rates for the non-detections are quoted as 90% confidence upper limits.

GJ	Obs. type	Obs.seq.	Filter	Exp. Time[a] (s)	Sep.[b] (')	Net Counts	Count rate[c] (ct/ks)	Error[d]	Signif.	CF[e]
398	survey	–	S1	1381	–	<10.4	<7.5	–	–	1.3
398	survey	–	S2	1459	2.1	13.4	10.1	4.7	3.2	1.1
398	pointed	201724	S2	601	–	<2.3	<19.4	–	–	5.3
406	survey	–	S1	1240	–	<20.9	<16.8	–	–	1.3
406	survey	–	S2	1723	0.7	53.1	33.9	7.1	7.1	1.1
406	pointed	201722	S2	2248	1.6	11.9	27.3	11.9	3.4	5.3
406	pointed	201577	S2	1232	–	<9.3	<37.4	–	–	5.3
845	survey	–	S1	1610	1.6	18.3	12.5	4.3	4.4	1.1
845	survey	–	S2	1247	–	<26.8	<21.5	–	–	1.1
845	pointed	200559	S2	10499	1.6	43.7	20.9	5.9	4.6	5.4
866	pointed	201723	S2	6718	–	<18.9	<14.4	–	–	5.3
887	pointed	201339	S2	13424	0.7	31.0	11.6	4.1	3.8	5.3

[a]. Due to differing instrument constraints, the exposure times for WFC and PSPC (cf. Table 2) are not necessarily the same.
[b]. Optical - EUV separation (arcmin).
[c]. WFC count rate, corrected to on-axis, 'at-launch' value (cf. Pye et al. 1995).
[d]. 1 standard deviation error.
[e]. Correction factor for decrease in photon detection efficiency of the WFC with time (cf. Pye et al. 1995). CF is the ratio of photon detection efficiency at launch to that at the time of the observation.

tail stars showing variability during the ROSAT X-ray observations. Long term variability between IPC and PSPC observations, will be discussed later, after having discussed the spectral characteristics, crucial for cross-calibrating the two instruments. In the following discussion we have included all photons with energy in the (0.11-2.4) keV passband.

3.1. GJ 191

This star, also called Kapteyn's star, is the only halo star in our sample with enough counts to allow us to study (cf. Fig. 1) its X-ray variability. This star has been observed twice six months apart, allowing us to study the variability on time scales of a few days and six months.

The first observation has a total observation time of $\sim$ 15 ks spanning one day. The light curve is consistent with that of a constant source. The second observation

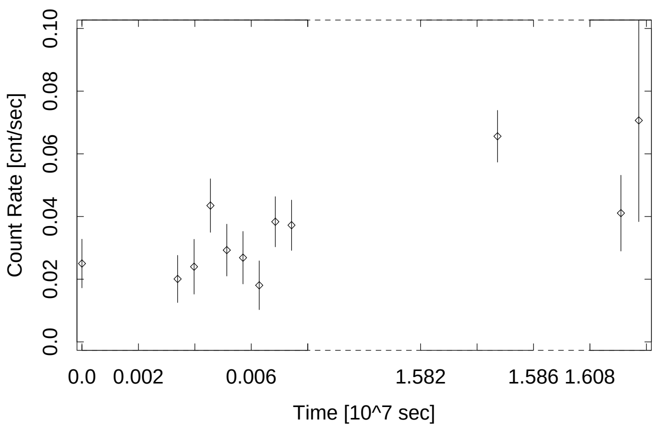

Fig. 1. X-ray light curve of the star GJ 191. Times are measured from the beginning of first observation (Obs. seq. 200523). Note the big gaps along the time axis.

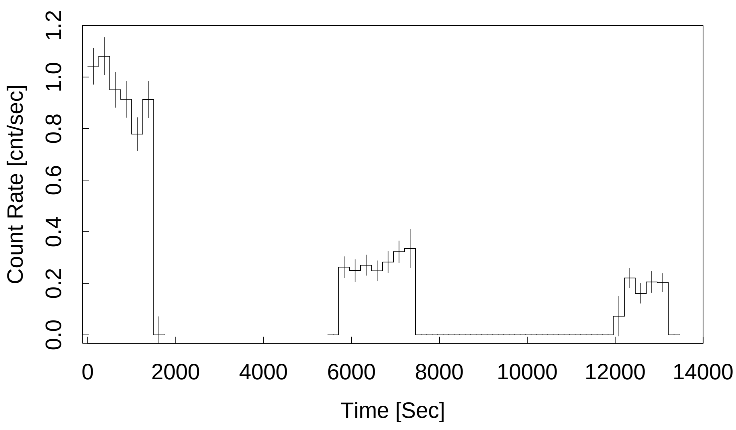

Fig. 2. Light curve of the star GJ 406 with a temporal bin of 250 s. Times are measured from the beginning of the first observation (Obs. seq. 201577)

is $\sim$ 3 ks long with 2.14 ks taken in a single day and the remaining time spanning two hours two days later. The mean rate observed is twice that observed six months before. Looking at the light curve it is evident that this increase of the X-ray luminosity is mainly concentrated in the first segment of this observation where the observed rate is 0.066 cnt/s $\pm$8.5%, while the rate in the second segment is 0.048 cnt/s $\pm$15%, marginally consistent with the rate observed six months before. Given the shortness of this observation we are unable to discriminate if the observed variability is due to flare occurrence or to other phenomena, influencing the coronal emission of this star.

3.2. GJ 406

The star GJ 406 (CN Leo) has been observed from two observers on the same day for a total time of $\sim$ 4.2 ks spanning less than four hours. Figure 2 shows the complete light curve. The star shows a flare with a peak value at least five times greater than the "quiescent" value measured at the end of the observation. Due to temporal gaps we do not have a good coverage of the decay phase and cannot directly measure the decay time that, in any case, is expected to be in the 2000-3000 s range. The occurrence of this flare explains the high value of L_x reported by Schmitt et al. (1995) who had available only the first time segment reported in Fig. 2.

We note that Ambruster et al. (1987) reported in their systematic study of X-ray variability of nearby dM stars observed by *Einstein* that CN Leo shows variability on time scales of hundreds of seconds with an amplitude of the order of 50%. They interpreted this variability as due to the presence of a small flare occurring at the end of the observation performed on 21-05-79. The second IPC observation (on 5-12-79) with only 80 counts, is consistent with the coronal emission being constant.

3.3. GJ 845

GJ 845, the only K star in our sample, is also the X-ray brightest source among the stars we are considering, and has been selected because is the only old star for which it has been possible to fit the X-ray spectrum obtained with the *Einstein* IPC (Schmitt et al. 1990). Hence we can use it for comparison among the two instruments. The PSPC observation of GJ 845 is $\sim$ 15 ks long, spanning a total time of $\sim$ 12 days. The first $\sim$ 4.5 ks were obtained during the first 4 hours of the observation, after $\sim$ 7 days other 1.6 ks were obtained, while the remaining observation time was allocated during the last two days. The light curve shown in Fig. 3 shows variability on many time scales, with an evident flare at the beginning of the 10-th day of observation with an increase of the luminosity in the PSPC of at least a factor two. During the first day of observation the star shows a low emission level with some indication of variability at a time scale of some thousands of seconds. After 7 days the count rate is slightly increased, with a larger increase occurring after 10 days. After the flare occurrence the rate seems to return to this "high" quiescent level. The change in the quiescent level could be due to rotational modulation. The observational gaps do not allow us to estimate the time scale of the decay of the flare, but only to put an upper limit of $\sim$ 6000 s on it.

3.4. GJ 866

The star GJ 866 has been observed for $\sim$ 13.2 ks spanning a total time of 13.2 hours. The light curve is shown in Fig. 4. We have defined the quiescent value as the mode of the distribution of the individual bin rates, corresponding to $\sim$ 0.20 cnt/s. The figure shows, just at the end of the observation, the beginning of a flare with the emission increasing at least by a factor 10 with respect to the qui-

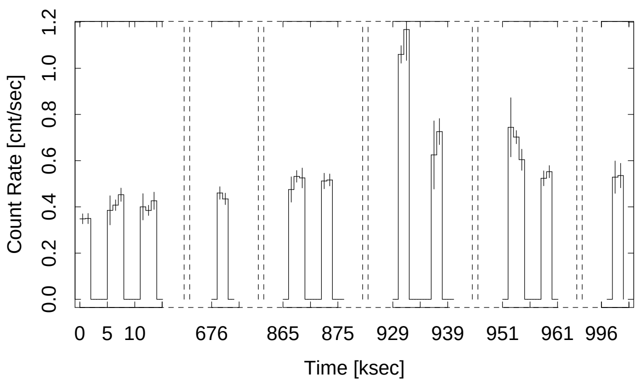

Fig. 3. Light curve of the star GJ 845 with a temporal bin of 1000 s. Times are measured from the beginning of the observation. Note the big gaps (indicated by dashed lines) along the abscissa

escent value. Unfortunately we cannot observe either the peak or the decay time of the flare. Furthermore the light curve shows an increase in the emission of a factor ~ 2 during the observation time between 28,000 and 30,000 s. There is indication of other short term variability at the beginning of the observation and at around 12,000 s.

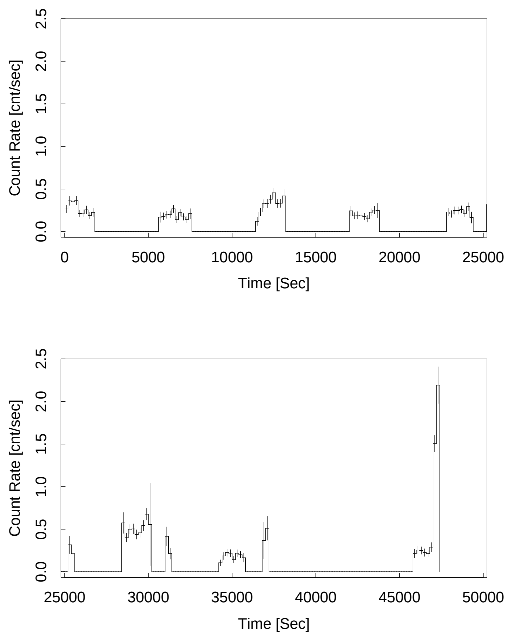

Fig. 4. Light curve of the star GJ 866 with a temporal bin of 200 s. Times are measured from the beginning of the observation.

GJ 866 was observed by the IPC twice, on May, 10, 1980 and May 12-13, 1980. Ambruster et al. (1987) find that during the first observation the X-ray emission of the star shows variability at a high significance level, probably due to decay of a flare at the beginning of the observation, while the quiescent emission is consistent with the level observed during the second observation.

The star is a binary system with two components of similar spectral type. The distance between the two components is 1.22 AU and the orbital period is 2.2 ± 0.02 yr (Leinert et al. 1990). Both the IPC and the PSPC observations observed the star at a similar orbital phase.

3.5. GJ 887

This star has been observed for $\sim$ 13.5 ks spanning a day. The light curve, shown in Fig. 5, shows variability of a factor $\sim$ 2 between the last $\sim$ 3 ks and the remaining observation. In this case we cannot decide whether the observed variability is due to flaring or to appearance of bright coronal structures.

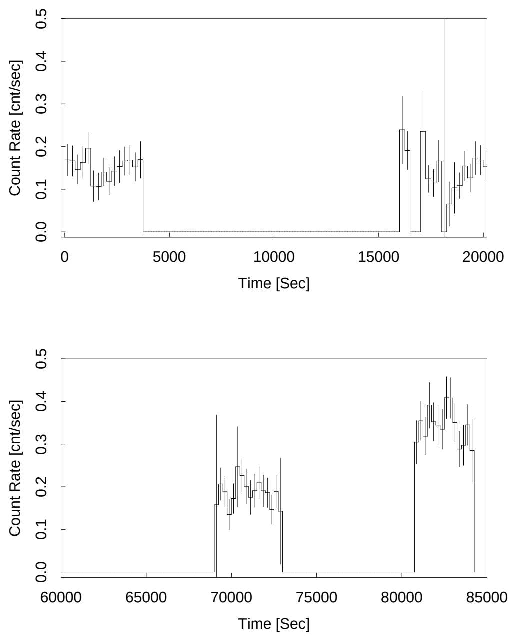

Fig. 5. Light curve of the star GJ 887 with a bin of 250 s. Times are measured from the beginning of the observation.

This star has been observed by the IPC but with not enough counts to perform variability analysis.

4. X-ray Spectra and Luminosity

We have evaluated the hardness ratio defined as $\mathrm{HR} = \frac{\mathrm{H-S}}{\mathrm{H+S}}$ where S are photons measured in channels 3-10 (0.11-0.42) keV, while H are photons recorded in channels 11-30 (0.42-2.4) keV. With this definition, following the recipe of Schmitt et al. (1995), we have computed the conversion factor from counts to flux to evaluate the X-ray luminosity in the (0.1-2.4) keV band. Resulting flux and luminosity are reported in Table 4. Upper limits for undetected stars have been evaluated assuming a conversion factor corresponding to the mean of those adopted for detected stars.

Table 4. Hardness ratio, X-ray fluxes and luminosities averaged during the entire observations

GJ	HR	Conv. factor	Rate (ct/ks)	f_x (erg/s/cm^2)	log L_x (erg/s)
1	-0.658	4.8e-12	20.86	1.01e-13	26.39
191(1)	-0.712	4.5e-12	29.27	1.33e-13	26.38
191(2)	-0.607	5.1e-12	60.50	3.08e-13	26.74
213	-0.886	3.6e-12	7.23	2.61e-14	26.05
299	...	(5.3e-12)	<5.68	<2.92e-14	<26.20
398	-0.066	8.0e-12	233.33	1.86e-12	28.62
406(1)	-0.173	7.4e-12	1001.67	7.41e-12	27.71
406(2)	-0.173	7.4e-12	267.59	2.28e-12	27.19
595	...	(5.3e-12)	<5.24	<2.69e-14	<26.42
699	-1.000	3.0e-12	23.34	7.03e-14	25.45
821	-0.705	4.6e-12	6.63	3.03e-14	26.63
845	-0.591	5.2e-12	578.50	3.00e-12	27.63
866	-0.335	6.5e-12	327.52	2.14e-12	27.47
887	-0.565	5.3e-12	230.65	1.23e-12	27.26

1, and 2 in parenthesis indicate, for the stars observed twice, the earlier and later observations.
Values of upper limits are obtained assuming the mean values of conversion factors obtained for the other stars in our sample

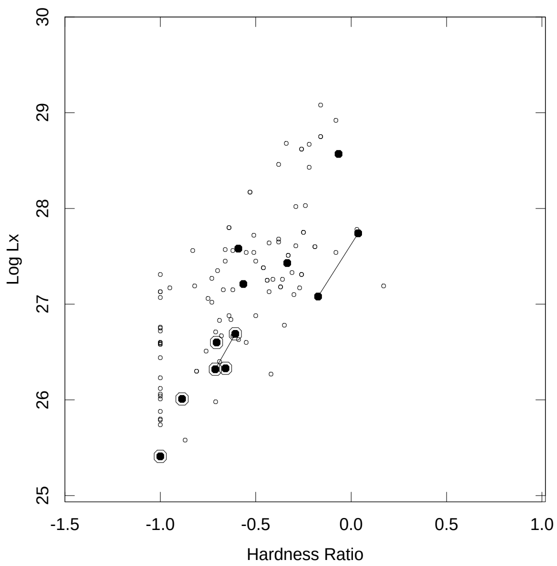

Fig. 6. Log L_x vs. Hardness Ratio for the low-mass stars in the solar neighborhood from Schmitt et al. (1995). Filled points indicate our data, points with big circles indicate the halo stars. Line joins two different observations of the same star. Note that halo stars systematically occupy the lower envelope defined by the nearby stars.

Figure 6 shows the scatter plot of L_x vs. HR for dK-dM stars inside 7 pc (adapted from Schmitt et al. 1995), the big symbols indicate our observations and big symbols with circles show our *H* or *O/H* stars. It is evident from this figure that Population II stars tend to occupy in this plane the lower envelope defined by nearby stars. Fleming et al. (1995) do not find any difference in this plane between the behavior of kinematically young and old disk stars in their sample. Indeed our old disk stars fall in the body of their distribution, while halo stars seem to congregate in the lower part of their data point envelope.

For all stars in our sample with enough count statistics we have performed spectral fits using the spectral package implemented in the Post-Reduction Off-line Software PROS V2.4 developed by the High Energy Astrophysical Division of the Smithsonian Astrophysical Observatory. We have fitted the spectra with 1-T and 2-T Raymond-Smith (Raymond & Smith 1977, Raymond 1988) models. In the adopted procedure the Gehrels (1986) approach for small number uncertainties is currently included. This allows to correctly treat weakly populated spectral bins. We have introduced a systematic error of 2% (cf. Fiore et al. 1995) required to allow for residual uncertainties in the "January 1993" PSPC response matrix. We have assumed for the emitting plasma, solar metallicity for all the stars except GJ 191; in this last case a different photospheric value is reported in the literature. Since the most intense sample stars are within 4 pc, we have neglected the presence of the hydrogen column. The ranges given for the fitted parameters, and reported in square brackets, are computed at the 99% confidence level considering two interesting parameters (see Avni, 1976 for a discussion on the concept of interesting parameters). All 1-T fits have 30 degrees of freedom (dof), while all 2-T fits have 28 dof, a fit has been considered unacceptable if the χ^2 results in a probability to reject the fit greater than 99%.

For the most intense stars, since they are all variable, we have considered spectra collected in different time intervals in order to explore the nature of the observed variability. Regrettably only one of the halo stars has enough count statistics to allow us to perform a meaningful spectral fit.

4.1. GJ 191

We have performed spectral fits separately for the two observations, adopting a value of metallicity, $z = 0.3$, according to the results of Mould (1976) and Cayrel de Strobel (1992). Assuming a simple single (1-T) temperature model, we obtain acceptable fits in both observations, with chi-square, $\chi^2 \sim 10$. The obtained temperature is in the [0.09-0.22] keV range and the logarithm of the emission measure is in the [49.23 - 49.61] cm^{-3} range in the first observation, while in the second observation the temperature is in [0.06 - 0.31] keV range and log(EM) in [49.36 - 49.96] cm^{-3} range. On the basis of these results, we cannot distinguish these two spectra, nor reject, on the basis of χ^2 value, the hypothesis that the emission originates from a 1-T plasma. However, we note that in the second observation, having a higher emission level, the observed counts in the 0.5-1.3 keV range show an excess with respect to the best-fit predicted ones that is significant at more than 4σ confidence level. A similar excess does not show up in the first observation. For this reason we have tried to fit the data of the second observation with a 2-T model, and the results show that we cannot exclude (but neither prove) the presence of a high temperature (at kT $>$ 0.5 keV) component with an emission measure comparable to that of the low temperature one.

Coming back to the adopted a value of $z = 0.3$, we notice that a change of metal abundance in a plasma with temperature $\sim 10^6$K, does not affect the temperature(s) obtained from fits to low resolution spectra, but only the resulting emission measure, since in this range of temperatures the emission is almost entirely due to emission lines, hence we obtain the same low-resolution spectrum decreasing the metal abundance and increasing at the same time the emission measure, maintaining constant the temperature.

4.2. GJ 406

We have separately performed the spectral fit for each of the three segments in which the star shows a different emission level. For all fits, according to photospheric measurements of Hartwick et al. (1984), we have adopted a plasma with solar metallicity. At the peak of the flare we have to reject the hypothesis that the plasma is dominated by 1-T component ($\chi^2 = 88.6$) and we have to invoke the presence of a high temperature component. The resulting 2-T fit yields $T_{low} = 0.16$ keV with an emission measure $\log(EM_{low}) = 49.73$ cm^{-3} and $T_{high} = 0.7$ [0.5 - 1.0] keV with $\log(EM_{high}) = 50.03$ [49.58 - 50.33] cm^{-3} ($\chi^2 = 23.4$).

In the other two segments of the observation, the 1-T fits are acceptable ($\chi^2 =$ 29.9 and 7.54, respectively). The resulting parameters are: T = 0.26 [0.215 - 0.32] keV and log(EM) = 49.72 [49.64 - 49.84] cm^{-3} for the first of these segments, and T = 0.23 [0.16 - 0.295] keV and log(EM) = 49.59 [49.34 - 49.74]cm^{-3} for the second. The spectrum collected in the last segment of the observation is modeled with a plasma slightly cooler and with a lower emission measure than the plasma we need to model the first one, but count statistics do not allow us to firmly reject the hypothesis that the plasma at these different times is in similar physical conditions. We have verified that the pattern of residuals resulting from 1-T fits, is consistent with a random one, and in no case do the residuals require a more complicate emission measure distribution.

4.3. GJ 845

The high rate of this source allows us to perform time resolved spectral analysis on a total of 11 different spectra, one for each observational interval. The results of the 1-T temperature fits are reported in Table 5. Excluding the fit in segment 7, corresponding to the peak of the flare, all the fits are statistically acceptable, but a visual inspection of the residuals reveals a systematic behavior, present essentially in all 11 spectra, with a deficit of observed counts with respect to the predicted ones in (0.4-0.7) keV and an excess above 0.8 keV. Furthermore there is a clear trend of an increase of the χ^2 with the increase in the number of collected counts. This suggests the presence of systematic errors we are neglecting or that the model is not a good representation of observed emission. The limited statistics of each single temporal bin do not allow us to unambiguously detect the presence of a high temperature component, whose presence is suggested by the systematic pattern in the residuals. In order to detect this high temperature component, we take advantage that in all temporal bins (except in the flare peak) the resulting fitted temperatures are very similar each to the other, suggesting that the observed variations in the light curve are mainly due to emission measure variations and not to temperature variations.

Table 5. Time resolved 1-T spectral fit for GJ 845 assuming solar abundance

#Segment	Collected Counts	T (keV)	log(EM) (cm^{-3})	χ^2 (30 d.o.f.)
1	763	0.17	50.09	7.70
2	848	0.16	50.13	27.84
3	722	0.15	50.09	14.07
4	846	0.17	50.21	18.52
5	900	0.17	50.25	20.32
6	834	0.17	50.24	19.86
7	1093	0.23	50.61	66.45
8	269	0.18	50.41	5.81
9	1088	0.20	50.41	36.74
10	928	0.18	50.28	28.27
11	268	0.19	50.30	11.03

Hence we have summed up all the spectra (with the exception of segment #7) and have performed the 1-T fit on the resulting spectrum, obtaining a $\chi^2 = 163.4$ making the fit unacceptable. The observed spectrum is shown in Fig. 7 (panel a) together with the "best" 1-T fit. In panel (b) of the same figure we report the residuals showing the typical behavior discussed above and that now, thanks to the higher statistics, allow us to firmly reject the assumed 1-T model.

On this basis we have performed a 2-T fit on the overall "quiet" observation obtaining a non-negligible high temperature component. The results of the fit are: $T_{low} = 0.13$

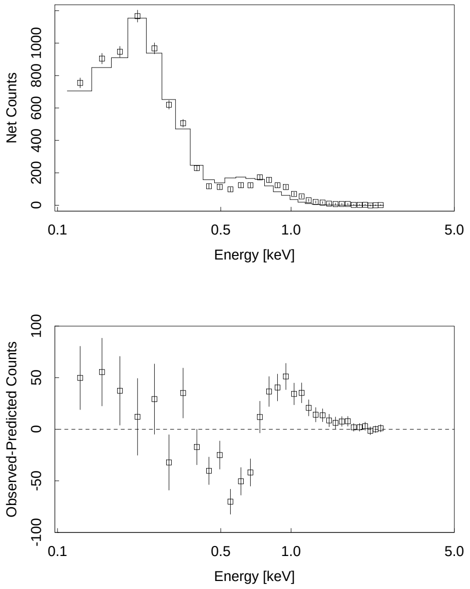

Fig. 7. 1-T fit (χ^2 = 163.4) for the quiescent phase of GJ 845 (upper panel) and the residuals (lower panel). Notice the systematic behavior of the residuals that mimic the pattern observed in each temporal bin.

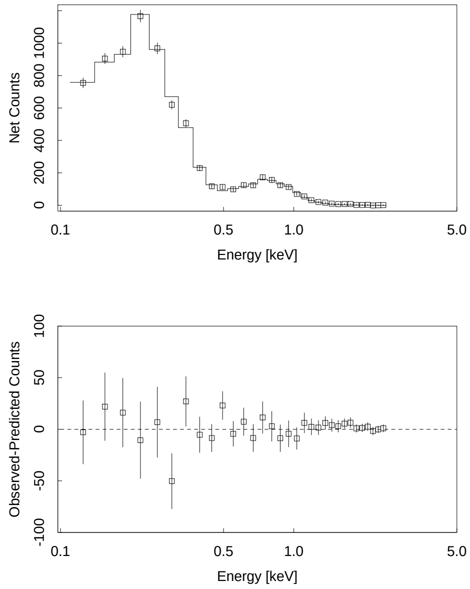

Fig. 8. Two-temperature fit (χ^2 = 17.75) for the quiescent phase of GJ 845 (upper panel) and the residuals (lower panel).

[0.1 - 0.15] keV with $\log(\mathrm{EM_{low}})$ = 50.06 cm^{-3}, and $\mathrm{T_{high}}$ = 0.41 [0.25 - 0.75] keV with $\log(\mathrm{EM_{high}})$ = 49.58 cm^{-3}, and χ^2 = 17.75. Figure 8 shows the results of the fit and the new residuals that now do not show any systematic behavior. The high temperature component has an emission measure $\sim$ 1/3 of that of the low-temperature component and this low value, together with the low value of the high temperature, is responsible for the difficulty in clearly detecting its presence with lower count statistics.

For the reason discussed above, instead of attempting to fit each temporal bin with a 2-T model, we have verified if our data are consistent with the hypothesis that the emission can be described by a 2-T model, with the two temperatures fixed at the values obtained by the fit of the overall "quiescent" phase, and with adjustable emission measures to fit the data. The resulting emission measures are shown in Table 6 together with the resulting χ^2. All segments of the observations are acceptably fitted by a such model (also the flare). At the bottom of the table we present the fitted emission measures obtained summing the spectra recorded in almost adjacent temporal bins and in which the emission does not show appreciable changes in intensity and spectrum. The resulting values of emission measures indicate that the low temperature component attains its lowest value at the beginning of the observation, increases by $\sim$ 25% at segment 5, maintaining this value up to the end of the observation, while during the flare it increases by $\sim$70% with respect to the initial value. The hot component also has its lowest level at the beginning of the observation; it increases by $\sim$ 60% at segment 5, by a factor $\sim$ 9 during the flare, and assumes a value $\sim$ 3 times greater that the initial value after the flare.

We have also fitted the peak flare emission with a 2-T model allowing both temperatures and emission measures to vary. In this case we obtain $\mathrm{T_{low}}$ = 0.18 [0.075 - 0.22] keV with $\log(\mathrm{EM_{low}})$ = 50.39 cm^{-3}, and $\mathrm{T_{high}}$ = 0.91 [0.4 - 1.8] keV with $\log(\mathrm{EM_{high}})$ = 50.33 cm^{-3} with χ^2 = 16.42. Both the low and high temperature intervals are consistent with the temperature range observed in the quiescent phase (likely because of the limited high temperature sensitivity of the PSPC), while the emission measure, in particular that of the high temperature component, increases significantly.

The IPC observation of this star (Schmitt et al. 1990) gave an acceptable 1-T fit with T = 0.22 keV and $\log(\mathrm{EM})$ = 49.8 cm^{-3}. This temperature is very similar to that obtained in our unacceptable 1-T fit and the emission measure is half of that we obtain. We have verified that at the lower spectral resolution and sensitivity of the IPC, the 1-T best fit produces an observed spectrum that is not distinguishable from that resulting from the 2-T fit we obtain with the PSPC.

4.4. GJ 866

The count statistics allow us to perform time resolved spectroscopy on the 11 time intervals shown in Fig. 4. For each interval we have fitted simple single temperature models to the observed spectrum. The results of these fits are reported in Table 7. They are very similar to those of

Table 6. Emission measures for G J845 assuming a 2-T model with $T_{low} = 0.13$ keV and $T_{high} = 0.41$ keV

#Segment	log(EM_{low}) (cm^{-3})	Conf. Intervals 99%	log(EM_{high}) (cm^{-3})	Conf. Intervals 99%	χ^2 (30 dof)	L_x (10^{27} erg/s)
1	49.94	49.85-50.00	49.26	48.45-49.55	8.4	2.52
2	50.00	49.95-50.10	49.37	48.85-49.55	20.8	2.96
3	50.01	49.95-50.10	49.27	48.55-49.55	6.30	2.86
4	50.05	49.95-50.10	49.45	48.95-49.75	13.93	3.36
5	50.10	50.00-50.17	49.55	49.15-49.75	8.86	3.88
6	50.10	50.03-50.17	49.51	49.05-49.85	11.24	3.76
7	50.23	50.12-50.30	50.28	50.15-50.35	26.60	9.21
8	50.19	50.00-50.35	49.83	48.65-50.05	4.36	5.43
9	50.12	50.03-50.17	49.93	49.75-50.05	24.65	5.42
10	50.07	50.00-50.15	49.69	49.15-49.85	12.38	4.11
11	50.07	49.85-50.15	49.71	48.65-49.95	10.07	4.17
1-3	49.99	49.95-50.05	49.33	49.20-49.45	12.57	2.81
5-6	50.10	50.05-50.15	49.53	49.35-49.65	16.81	3.83
8-11	50.10	50.05-50.15	49.83	49.75-49.95	22.55	4.85

GJ 845 with the 1-T fits yielding acceptable χ^2, although the fit of segments 7 and 11 are only marginally acceptable, but the patterns of the residuals suggest the presence of a low-emission measure higher temperature component. In order to verify its existence we have followed the same procedure adopted for GJ 845, fitting the counts recorded in all the observation excluding segments 7 and 11. We collect a total of 2721 counts. A 1-T fit yields a $\chi^2 = 101.6$ that allows us to reject the model.

Table 7. Time resolved 1-T spectral fit for GJ 866, assuming solar abundance

#Segment	Counts	T [keV]	log(EM) [cm^{-3}]	χ^2 (30 d.o.f.)
1	544	0.21	50.00	19.9
2	375	0.21	49.85	7.9
3	591	0.22	50.09	21.8
4	343	0.20	49.84	13.5
5	395	0.20	49.94	22.8
6	65	0.23	49.96	2.9
7	815	0.25	50.27	53.6
8	55	0.20	49.99	2.1
9	316	0.18	49.80	11.3
10	38	0.22	50.22	2.3
11	788	0.26	50.28	48.1

A 2-T fit yields an acceptable fit ($\chi^2 = 22.12$) with $T_{low} = 0.15$ [0.08 - 0.35] keV and log(EM_{low}) = 49.73 cm^{-3}, and $T_{high} = 0.57$ [0.4 - >5.0] keV and log(EM_{high}) = 49.37 cm^{-3}, without any systematic pattern in the observed residuals. We find that the emission of GJ 866 requires a high temperature component (with $EM_{high} < EM_{low}$) but the data prevent us from constraining its value. Finally, adopting a procedure similar to that for GJ 845, we have fitted data in each temporal bin, fixing the two temperatures at the value obtained by the best fit of the overall "quiescent" phase. The resulting emission measures and luminosities are reported in Table 8.

Again the observations are consistent with a description in terms of a 2-T model with the temperatures constant in time and emission measure variations responsible for the observed variability.

4.5. GJ 887

For GJ 887 we have adopted an approach similar to that used above. In this case we can separate the emission into four distinct time bins. 1-T fits give results similar to those of the other stars in our sample. Temperatures, emission measures and χ^2 are reported in Table 9. Also in this case the χ^2 values result in statistically acceptable fits, but the residuals show a systematic pattern.

To further outline the observed behavior of the residuals we have summed up the counts collected in segments 1, 2, and 3, where the best fits have similar parameters, obtaining a total of 1870 counts. In this case the 1-T fit gives a $\chi^2 = 52.44$ allowing us to reject the model. A 2-T fit gives $\chi^2 = 10.89$ with $T_{low} = 0.13$ [0.1 - 0.16] keV, log(EM_{low}) = 49.63 cm^{-3}, $T_{high} = 0.53$ [0.25 - 1.0] keV, and log(EM_{high}) = 49.0 cm^{-3}. We have verified that the emission in each time interval is consistent with these parameters. The results, reported in Table 10, are analogous to those obtained for the other stars.

A 2-T fit with the two temperatures considered free parameters in segment 4 (where 1-T fit is not acceptable) gives $T_{low} = 0.15$, $T_{high} = 0.72$, log(EM_{low}) = 49.93 cm^{-3}, and log(EM_{high}) = 49.60 cm^{-3}, consistent with the parameters reported in Table 10.

Table 8. Emission measures for GJ 866 assuming a 2-T model with $T_{low} = 0.15$ keV and $T_{high} = 0.57$ keV

#Segment	$\log(EM_{low})$ (cm^{-3})	Conf. Intervals 99%	$\log(EM_{high})$ (cm^{-3})	Conf. Intervals 99%	χ^2 (30 dof)	L_x (10^{27} erg/s)
1	49.79	49.64-49.89	49.41	48.99-49.74	13.6	2.37
2	49.65	49.49-49.74	49.20	48.55-49.60	8.4	1.60
3	49.83	49.69-49.89	49.57	49.33-49.83	13.4	2.91
4	49.66	49.49-49.79	49.18	48.46-49.61	10.5	1.63
5	49.75	49.59-49.84	49.37	48.85-49.70	10.2	2.16
6	...	...	...	...	...	...
7	49.92	49.79-50.04	49.87	49.62-49.97	25.4	4.58
8	...	...	...	...	...	...
9	49.68	49.54-49.79	49.03	<47.68-49.48	7.7	1.53
10	...	...	...	...	...	...
11	49.92	49.79-50.04	49.89	49.62-49.87	17.8	4.71

The time intervals 6, 8, and 10 have not been considered given their low count statistics.

Table 9. Time resolved 1-T spectral fit for GJ 887

#Segment	Counts	T [keV]	log(EM) [cm^{-3}]	χ^2 (30 d.o.f.)
1	625	0.18	49.76	14.4
2	529	0.16	49.72	17.5
3	716	0.16	49.81	28.1
4	1245	0.20	50.12	63.0

5. Discussion

5.1. X-Ray Luminosity

Stars defined as H or OH in our sample show an emission level lower than that shown by the OD stars. The typical range of luminosity for H and OH stars is $10^{26} - 5 \times 10^{26}$ erg/s, with the extremely low value of $\sim 3 \times 10^{25}$ erg/s for GJ 699. The OD stars have an emission level variable up to typically a factor 3-4 with values in the $10^{27} - 9 \times 10^{27}$ erg/s range, well above the value observed for the Halo stars. The range of luminosity of Halo stars is in the low tail of the X-ray luminosity function obtained by Barbera et al. (1993) and Schmitt et al. (1995) for the nearby dK and dM stars, while the range of luminosity of the Old disk stars is around the median. We note the star GJ 398 that is in the high luminosity tail of the X-ray luminosity function, has a space velocity very similar to that of the young disk population stars.

The stars for which we have been able to perform time resolved spectral fits, namely the three OD stars GJ 845, GJ866, and GJ887, have shown a common behavior with similar temperatures, with T_{low} and T_{high} in the 0.13-0.15 keV, and in 0.4-0.57 keV ranges, respectively, and variable emission measures. In Fig. 9 we plot the emission measure of the high temperature component versus the emission measure of the low-temperature plasma for all the time intervals considered for the three stars, each represented with a different symbol. This plot shows a well defined relation between the two emission measures with a law:

$$\log(EM_{high}) = A + B \log(EM_{low})$$

where the slope B is about 3 for all the observed stars, while A is a property characteristic of each star, and, considering that GJ 845 is the only K star we are considering, may depend on stellar mass (or radius). This result suggests that, at least for the OD low-mass stars, the plasma emitting at the different temperatures is related and that the variations of density of plasma at different temperature are interrelated. This behavior could be explained if the emission responsible for the variations originates on a few active regions, containing two dominant classes of loops, each "corresponding" to one of the fitted temperatures, changing coherently with the emergence of magnetic flux on the stellar surface. Our data suggest that the classes of dominant loops and their response to variations of heating mechanism are similar in the class of old late-type stars. The value of A is related to the "quiescent" status of the star, and it is probably, a measure of the density and/or filling factor of the active regions on the stellar surface. The same basic idea would still be valid even if our 2-T model simply reflects an actual emission-measure distribution that is continuous with temperature, with the 2-T fit resulting from the limited spectral capabilities of the instrumentation (e.g. Majer et al. 1986; Schmitt et al. 1987).

The observed changes in emission measures, with essentially constant temperatures, imply both changes in the shape of stellar coronal spectrum, hence in the observed hardness ratio, and in the measured X-ray luminosity. We would therefore expect that the behavior of the three more intense sources of our sample observed in Fig. 9 should be observed in a similar way in the L_x – HR plane, (cf Fig. 6).

In Fig. 10 we show the value of HR and L_x measured in each time interval for GJ 845, GJ 866, and GJ 887, together with the values observed in the single observations

Table 10. Emission measures for GJ 887 assuming a 2-T model with $T_{low} = 0.13$ keV and $T_{high} = 0.53$ keV

#Segment	$\log(EM_{low})$ (cm^{-3})	Conf. Intervals 99%	$\log(EM_{high})$ (cm^{-3})	Conf. Intervals 99%	χ^2 (30 dof)	L_x (10^{27} erg/s)
1	49.59	49.50-49.67	49.02	48.59-49.24	5.1	2.24
2	49.58	49.47-49.67	48.88	48.08-49.18	15.3	1.13
3	49.70	49.62-49.67	49.03	48.55-49.30	11.7	1.50
4	49.86	49.79-49.92	49.61	48.46-49.76	18.3	3.02

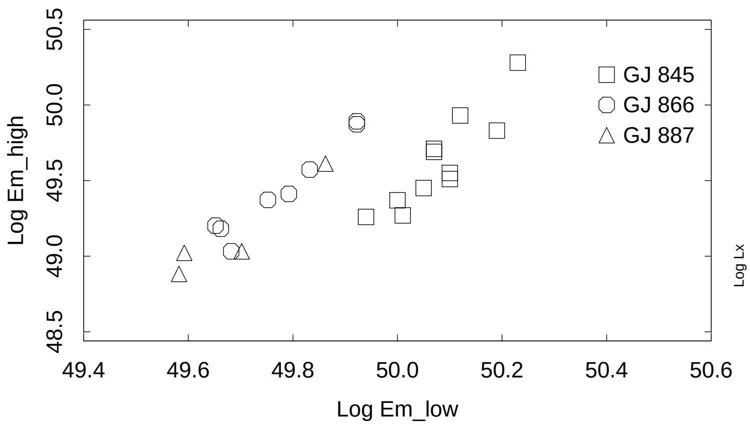

Fig. 9. Emission measure of the high temperature component versus the emission measure of the low-temperature one for different time intervals for the three more intense OD stars, represented by different symbols as in legend.

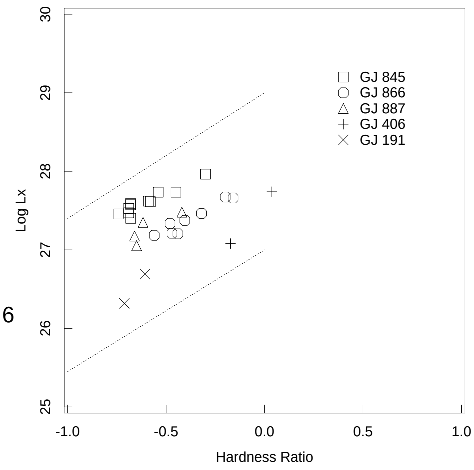

Fig. 10. Scatter plot of L_x vs. HR at different observational time intervals for the more intense sources of our sample. The two dashed lines indicate the region occupied by the nearest dK and dM stars (Schmitt et al. 1995).

of the stars GJ 191 and GJ406. The two dashed lines indicate the region occupied by the stars in the sample of Schmitt et al. (1995). This plot shows that also in this plane each star can move on a line with a slope similar for all stars, while the normalization can vary up to two orders of magnitude and depends on the given star.

5.2. Time variability

5.2.1. One-three year time scale variability

Schmitt et al. (1995) report on RASS measurements for about half of the stars in our sample. The comparison between the two measurements allows us to assess the presence of variability on time scales of 1-3 years that is the typical time between the RASS and our pointed observations.

Figure 11 reports RASS count rates obtained from Schmitt et al. (1995), vs. our deduced rates. The two lines correspond to variations of 50%. It is clear that variations larger than this value are typical for these stars on time scales up to few years (including the occurency of flares).

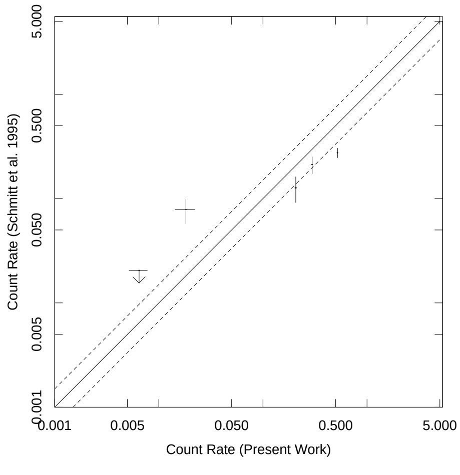

Fig. 11. Comparison of count rates in the present paper and in Schmitt et al. (1995). The solid line denotes equality of count rates in the two works, and the two lines delineate variations by 50%.

5.2.2. Long-Term variability

We have compared X-ray luminosities measured in our survey with those obtained with the IPC more than 10 years before. To cross calibrate the two instruments we have computed the conversion factor from IPC count rates to flux in the (0.1-2.4) keV PSPC bandpass assuming 1-T spectra with temperatures corresponding to the range of the HR values obtained in our PSPC observations. With this procedure we obtain an uncertainty in the count to flux conversion of $\sim$ 50%, hence we cannot consider significant variations smaller than this value. In Table 11 we report X-ray luminosities obtained with the two instruments. For the PSPC we report the values of luminosity from Table 2, for those stars for which we have obtained time resolved spectral analysis we report the range of observed L_x due to the short term variability. For the IPC we report the range of luminosity observed if more than one IPC observation is available, and the range due to the uncertainty in count to flux conversion, if only one observation exists.

Table 11. X-ray luminosities observed with IPC and PSPC

Name	$\log L_x$ (IPC)	Date of IPC observation(s)	$\log L_x$ (PSPC)
GJ 191	< 26.37-26.53	09/26/79	26.38-26.74
GJ 213	27.04-27.21	03/27/79	26.05
GJ 398	28.33-28.50	12/13/80	28.62
GJ 406	26.40-27.10	05/21/79-12/05/79	27.19-27.71
GJ 699	< 25.78-25.95	09/26/79	25.45
GJ 845	27.13-27.30	04/23/80	27.40-27.96
GJ 866	27.06-27.23	05/10/80-05/12/80	27.18-27.67
GJ 887	26.57-27.74	06/02/80	27.05-27.48

About half of the stars have luminosity values consistent in the two epochs, while the other half show variations of more than a factor two. Since variations of similar amplitude are observed on time scales of 1-3 years (see section above), we cannot discriminate if the observed variability on the scale of a decade reflects this shorter time variability or suggests the existence of a solar-like cycle. Only for the star GJ 213 is the observed variation as high as about one order of magnitude, much larger than the variations observed on shorter time scales in our stars. Furthermore, based on examination of the IPC light curve, we can confidently exclude that the IPC observation of this star has been obtained during a big flare. To the best of our knowledge this is the first halo star in which X-ray observations show evidence of long-term X-ray variability of an amplitude similar to that observed on the Sun.

6. Summary and conclusions

We have reported on the analysis of a sample of Halo and Old Disk low-mass stars observed with the ROSAT PSPC and WFC. All the stars with enough count statistics present variations of 50% and greater on time scales from hours to $\sim$ 1 day. The star GJ 191 observed with a time interval of $\sim$ 6 months shows variations of similar amplitude. Comparison of our observations with those of the RASS reported by Schmitt et al. (1995) indicates that similar variations are observed also on time scales of a few years. Finally, comparison between IPC and PSPC observations show evidence of long-term variation on the halo star GJ 213.

Spectra of the more intense sources show that the emission of these old stars may be described in terms of the emission from a 2-T plasma model with the cool component at $T_{low} \sim 0.15$ keV and the high temperature component at $T_{high} \sim 0.5$ keV, much lower than the typical high temperature reported for more active stars (see for example Schmitt et al. 1990, Kürster & Schmitt 1996, Ottmann & Schmitt 1994). Furthermore, in contrast with most of the active stars, the emission measure of the plasma at high temperature is smaller than the emission measure of the cool component. An analogous result have been found by Güdel et al. (1996) among a sample of nearby G0-G5 V, not too old stars.

We found that the coronal emission of our sample stars is consistent with a description in terms of a 2-T model with (approximately) constant values of the two temperatures along the entire observation, while the observed variability can be explained by changes in the emission measures. We found that in our sample stars the emission measure of the high-temperature component always changes coherently with that of the low-temperature component, but with a substantially larger change. The changes occur in such a way as to constrain the stellar coronal emission to describe an approximately linear locus in $\log(EM_{low})$-$-\log(EM_{high})$ plane (or analogously in $HR - L_x$ plane). We do not know if this behavior is typical of all the late-type stars or is characteristic only of the old, and hence relatively quiet stars in which the emission is expected to come from a few active regions. Similar EM_{high}/EM_{low} comparisons for BY Dra, RS CVn and W UMa systems are reported by Dempsey et al. (1993, 1994) and McGale et al. (1996). In those papers however, the plots are single points for each star, rather than sampling each star's lightcurve. (Hence we have to make the assumption that it is valid to compare multiple samples from a given star during different activity levels with single observations of a sample of stars where each one, in general, is exhibiting a different activity level.) There are (at least) two relations of interest: (i) the log-slope B (c.f. Section 5.1); (ii) the ratio EM_{high}/EM_{low}. The log-slope B for our 'old' M stars is much steeper than found for the more active stars, but the actual EM_{high}/EM_{low} ratio is much less. This is supported by examining the results of McGale et al. (1996) for SW Lac, W UMa and VW Cep where those authors performed spectral fits sampling the lightcurve. The first two stars show a log-slope $B \sim 1$, though the last is somewhat steeper, at $B \sim$ 2–3 (but does include a flaring episode). A systematic study on active stars including young-disk late-type stars is required to clarify this issue.

Acknowledgements. G.M. and S.S. acknowledge financial support from ASI (Italian Space Agency), and MURST (Ministero della Università e della Ricerca Scientifica e Tecnologica). J.P. acknowledges the financial support of the UK Particle Physics and Astronomy Research Council. This research has made use of the Simbad database, operated at CDS, Strasbourg, France.

References

Ambruster, C., Sciortino, S., Golub, L. 1987, ApJS, 65, 273

Avni, Y. 1976, ApJ, 210, 642

Barbera, M., Micela, G., Sciortino, S., Harnden, F. R., Jr. & Rosner, R. 1993, ApJ, 414, 846

Cayrel de Strobel, G., Hauck, B., Francois, P., et al. 1992, A&AS, 95, 273

Dempsey, R. C., Linsky, J. L., Fleming, T. A., & Schmitt, J. H. M. M. 1994, in Caillault, J.-P., ed., Cool Stars, Stellar Systems, and the Sun. ASP COnf. Ser., 64, 74.

Dempsey, R. C., Linsky, J. L., Schmitt, J. H. M. M., & Fleming, T. A. 1993, ApJ, 413, 333.

Feigelson, E. D., & Kriss, G. A. 1989, ApJ, 338, 262

Fiore, F., Elvis, M., Siemiginowska, A., et al. 1995, ApJ, 449, 74

Fleming, T. A., Schmitt, J. H. M. M., & Giampapa, M. S. 1995, ApJ, 405, 401

Gehrels, N. 1986, ApJ, 303, 336

Güdel, M., Schmitt, J.H.M.M., & Benz, A. O. 1995, A&A, 293, L49

Güdel, M., Guinan, E. F., Skineer, S. L. 1996, A&A, submitted

Hartwick, F. D. A., Cowley, A. P., & Mould, J. R. 1984, ApJ, 286, 269

Kashyap, V., Rosner, R., Micela, G., et al. 1992, ApJ, 391, 667

Kürster, M. & Schmitt, J.H.M.M. 1996, A&A, 311, 211

Leggett, S. K. 1992, ApJS, 82, 351

Leinert, Ch., Haas, M., Allard, F., et al. 1990, A&A, 236, 399

Linsky, J. L. 1985, Sol. Phys., 100, 333

Maggio, A., Sciortino, S., Harnden, F. R., Jr. 1994, ApJ, 432, 701

Majer, P., Schmitt, J. H. M. M., Golub, L., Harnden, F. R., Jr., Rosner, R., 1986 ApJ, 300, 360

McGale, P. A., Pye, J. P., Barber, C. R., Page, C. G., 1995, MNRAS, 275, 1232

McGale, P. A., Pye, J. P., & Hodgkin, S. T. 1996, MNRAS, 280, 627.

Mewe, R., Gronenschild, E.H.B.M, Heise, J., et al., 1982, ApJ, 260, 233

Micela, G., Sciortino, S., Serio, S. et al. 1985, ApJ, 292, 172

Micela, G., Sciortino, S., Vaiana, G. S., et al. 1988, ApJ, 325, 798

Micela, G., Sciortino, S., Vaiana, G. S., et al. 1990, ApJ, 451, 392

Micela, G., 1991, Ph. D. Thesis, University of Palermo

Micela, G., Harnden, F. R., Jr., Rosner, R., Sciortino, S., Vaiana, G. S., 1991, ApJ, 380, 495.

Micela, G., Sciortino, S., Kashyap, V., Harnden, F. R., Jr., Rosner, R., 1996, ApJS, 102, 75

Mould, J. R., 1976 ApJ, 210, 402

Nousek, J. A., & Lesser, A. 1993, Rosat Newsletter, 8, 13

Ottmann, R., & Schmitt, J. H. M. M. 1994, 283, 871

Pallavicini, R., 1989, A&Ap. Rev., 1, 177

Pallavicini, R., Monsignori Fossi, B. C., Landini, M., & Schmitt, J.H.M.M. 1988, A&A, 191, 109

Patten, B. M. & Simon, T. 1993, ApJ, 415, L23

Pye, J. P., Hodgkin, S. T., Stern, R. A., & Stauffer, J. R. 1994, MNRAS, 266, 798

Pye, J. P., McGale, P. A., Allan, D. J., et al., 1995, MNRAS, 274, 1165

Randich, S. & Schmitt, J.H.M.M. 1995, A&A, 298, 115

Randich, S., Schmitt, J.H.M.M., Prosser, C. F., & Stauffer, J. R. 1995a, A&A, 300, 134

Randich, S., Schmitt, J.H.M.M., Prosser, C. F., & Stauffer, J. R. 1995b, A&A, 303, 322

Raymond, J., & Smith, B. W. 1977, ApJS, 35, 419

Raymond, J. 1988, in Hot and Thin Plasmas in Astrophysics, ed. R. Pallavicini, Kluwer Academic Publisher, 3

Rosner, R., Golub, L., Vaiana, G., S., 1985, ARAA, 23, 413

Schmitt, J. H. M. M., Collura, A., Sciortino, S., et al. 1990, ApJ, 365, 704

Schmitt, J. H. M. M., Pallavicini, R., Monsignori-Fossi, B. C., & Harnden, F. R., Jr., 1987, A&A, 179, 193

Schmitt, J. H. M. M., Fleming, T. A., & Giampapa, M. S. 1995, ApJ, 450, 392

Sciortino, S., 1993, in "Physics of Stellar and Solar Coronae", Linsky, J., & Serio, S., eds., Kluwer, 211.

Stauffer, J. R., Caillault, J-P., Gagné, M., Prosser, C. F., & Hartmann, L. W. 1994, ApJS, 91, 625

Stern, R. A., Antiochos, S. K., & Harnden, F. R., Jr., 1986, ApJ., 305, 417

Stern, R. A., Schmitt, J. H. M. M., & Kahabka, P. T. 1995, ApJ, 448, 683

Vaiana, G. S., Fabbiano, G., Giacconi, R. et al. 1981, ApJ, 245, 163

Vaiana, G. S. 1983, in Solar and Stellar Magnetic Fields. Origins and Coronal Effects, ed. O. Stenflo (Dordrecht:Reidel), p. 165

Wood, B. E., Brown, A., Linsky, J. L., et al., 1994, ApJS, 93, 287

This article was processed by the author using Springer-Verlag LaTeX A&A style file *L-AA* version 3.